Applied Catalysis B: Environmental 219 (2017) 200–208

Contents lists available at ScienceDirect

Applied Catalysis B: Environmental

journal homepage: www.elsevier.com/locate/apcatb

Complete oxidation of formaldehyde at room temperature over an Al-rich Beta zeolite supported platinum catalyst

Ling Zhang[a], Long Chen[b], Yaobin Li[c], Yuexin Peng[a], Fang Chen[a], Liang Wang[a], Changbin Zhang[c], Xiangju Meng[a,*], Hong He[c], Feng-Shou Xiao[a,*]

[a] Key Lab of Applied Chemistry of Zhejiang Province, Department of Chemistry, Zhejiang University, Hangzhou, 310007, PR China
[b] Faculty of Chemistry Biology and Materials Science, East China Institute of Technology, Fuzhou 344000, PR China
[c] Research Center for Eco-Environmental Sciences, Chinese Academy of Sciences, Shuangqing Road 18, Beijing, 100085, PR China

ARTICLE INFO

Article history:
Received 17 January 2017
Received in revised form 4 July 2017
Accepted 7 July 2017
Available online 8 July 2017

Keywords:
Formaldehyde
Complete oxidation
Room temperature
Al-rich Beta zeolite

ABSTRACT

For human health and environmental protection, removal of formaldehyde (HCHO) has become a hot topic, and completely catalytic oxidation at room temperature has been identified as one of the efficient routes for solving this problem. Recently, it has been reported that zeolite-supported Pt catalysts are active for HCHO oxidation at low temperatures, but they are still unable to completely oxidize HCHO at room temperature. To enhance the activity, it has been suggested to increase the Pt dispersion and acidic density in the zeolite-supported Pt catalysts. We therefore chose Al-rich Beta as a zeolite support because abundant aluminum species in the zeolite framework are advantageous for increasing acidic density through ion-exchange of protons and for improving Pt metal dispersion through the metal-zeolite interaction by increasing the negative charge of the zeolite framework with positively charged metal ions. As we expected, the Al-rich Beta zeolite supported platinum catalyst is very active, giving complete oxidation of HCHO at room temperature. To the best of our knowledge, this is the first time the complete oxidation of HCHO at room temperature over a zeolite-supported noble metal catalyst has been realized. In addition to its extraordinary activity, this catalyst is also very stable and selective. The strategy of designing zeolite-supported noble metal catalysts might offer an alternative way to develop highly efficient heterogeneous catalysts for the removal of air pollutants.

1. Introduction

Formaldehyde (HCHO) is one of the major components of indoor air pollutants due to its broad applications in decorating and furnishing materials, which results in great threats to human health [1–14]. Therefore, the highly efficient removal of HCHO has been intensively studied in the past decades, and a series of techniques such as adsorption [15–18], photocatalysis [19–25], plasma technology [26–29] and catalytic oxidation [30–37] have been well developed. Among them, complete catalytic oxidation has been identified as one of the most efficient routes for HCHO abatement due to its non-toxic by-products and high activity at low temperatures [4,30,38–42]. Supported transition metal oxides and/or noble metals are the most useful catalysts for the catalytic oxidation of HCHO [30,38–55]. Compared with supported transition metal oxides, supported noble metals exhibit high activity [30,38–43,45,48–51,53,54]. Normally, titania [53,56–59], alumina [60–62] and silica [63–65] have been applied as supports for preparation of these noble metal catalysts, but recently, zeolite supports have received much attention for this oxidation, owing to their large surface areas, intricate channels, high adsorption capacity, adjustable acidic property, and high thermal and hydrothermal stabilities [66–70]. Notably, zeolite supported noble metal catalysts still show lower activities in the complete oxidation of HCHO than titania supported noble metal catalysts modified with alkaline cations [43,45,48,49,51,53,54,65]. Therefore, it is strongly desirable to develop highly efficient zeolite supported noble metal catalysts for the complete oxidation of HCHO at low temperatures, particularly at room temperature.

It has been reported that the presence of acidic sites is favorable for the oxidation of oxygenates at low temperatures [71] and enhancement of the metal-support interaction is helpful for high dispersion of the metal on the support [72,73]. Therefore, design strategies for improving activity in the complete oxidation of HCHO involve in increasing metal dispersion and acidic density in the zeolite supported noble metal catalysts.

* Corresponding authors.
E-mail addresses: mengxj@zju.edu.cn (X. Meng), fsxiao@zju.edu.cn (F.-S. Xiao).

http://dx.doi.org/10.1016/j.apcatb.2017.07.015
0926-3373/

To realize these strategies, we chose Al-rich Beta as the zeolite support [74–77] because abundant aluminum species in the zeolite framework are advantageous for increasing acidic density by ion-exchange of protons and for improving metal-zeolite interaction by increasing the negative charge of the zeolite framework with positively charged metals. As we expected, the Al-rich Beta zeolite supported platinum catalyst (Pt/H-Beta-SDS-4) shows complete oxidation of HCHO at room temperature. The catalysts were characterized by physical and chemical techniques, and their catalytic performance for HCHO oxidation was evaluated.

2. Experimental

2.1. Materials

$NaAlO_2$, formaldehyde solution, and NaOH were purchased from Sinopharm Chemical Reagent. Fumed silica (SiO_2) was obtained from Shenyang Chemical Co. Beta seeds (Si/Al at 12.50) were supplied from Nankai University Catalyst Co. Tetraethylammonium hydroxide solution (TEAOH, 2.0 M in H_2O) was obtained from BASF. $H_2PtCl_6{\cdot}6H_2O$, nitric acid, formic acid, and KNO_3 were purchased from Aladdin. All these materials were of analytical grade and used without further purification.

2.2. Preparation of catalysts

Synthesis of Beta-SDS and Beta-TEA: Seed-directed synthesis of Beta zeolite (Beta-SDS) was carried out in the presence of calcined Beta zeolite seeds. As a typical run, 3.2 g $NaAlO_2$ and 5.6 g NaOH were dissolved in 68 mL of H_2O, followed by addition of 20 g of fumed silica [75]. After stirring for 12 h, 1 g of Beta zeolite seeds were introduced into the gel, followed by stirring for 5 min. Then, the resulting gel was transferred into an autoclave for crystallization at 120 °C for 90 h. After filtering, washing with water at room temperature, and drying at 100 °C in air for 12 h, the solid product of Beta-SDS was finally obtained. The ICP-OES analysis of this Beta-SDS showed that the Si/Al ratio was 4.28. Therefore, this sample was designated as Beta-SDS-4.

Beta zeolite (Beta-TEA) was synthesized in the presence of TEA^+ cations. As a typical run, 1.5 g of $NaAlO_2$ and 0.8 g of NaOH were dissolved in 63 mL H_2O, followed by addition of 97 mL of TEAOH [78]. After stirring for 10 min, 24 g of fumed silica was introduced into the gel, followed by stirring for 12 h. Then, the resulting gel was transferred into an autoclave for crystallization at 140 °C for 96 h. After filtrating, washing with water at room temperature, drying at 100 °C in air for 12 h, and calcining at 550 °C for 5 h for removing the organic templates, the solid product of Beta-TEA was finally obtained. The ICP-OES analysis of this Beta-TEA showed that the Si/Al ratio was 11.67. Therefore, this sample was designated as Beta-TEA-12.

Beta-SDS samples with Si/Al ratios at 7.88 and 10.12 were prepared with acidic treatment of Beta-SDS-4 in 0.3 M HNO_3 and 0.6 M HNO_3 for 3 h, which were designated as Beta-SDS-8 and Beta-SDS-10.

The H^+-form of Beta-SDS (H-Beta-SDS) and Beta-TEA-12 (H-Beta-TEA-12) samples was prepared from NH_4^+-exchange of Na-Beta-SDS and Na-Beta-TEA-12, followed by calcination at 500 °C for 4 h. To decrease Na^+ concentration in the sample, the ion-exchange procedures were repeated for twice. Similarly, K-Beta-SDS-4 sample was ion-exchanged with KNO_3 solution (1 M) at 80 °C for 3 h for twice.

Preparation of zeolite Beta supported Pt catalysts: The zeolite Beta-supported Pt catalysts were prepared by an impregnation using an appropriate amount of aqueous solution of $H_2PtCl_6{\cdot}6H_2O$. After impregnation, the excessive water was removed in a rotary evaporator at 80 °C. The samples were dried at 120 °C for 12 h and then calcined at 400 °C for 4 h. The loading of Pt was 1.0 wt%.

2.3. Catalyst characterization

The crystalline structure of the samples was determined by a powder X-ray diffractometer (Rigaku Ultimate VI X-ray diffractometer) using Cu Kα (λ = 1.5406 Å) radiation at 40 kV and 40 mA with the step size of 0.065°(2θ).

A physisorption analyzer (Micromeritics ASAP 2020 M and Tristar system) was used to measure the surface area and pore structure (volume and size) of the samples by N_2 adsorption-desorption at 77 K. All samples were degassed at 90 °C for 12 h to remove the physisorbed moisture before the N_2 adsorption. The surface area was calculated from using the Brunauer-Emmett-Teller (BET) method.

The Si/Al ratios of Beta zeolites and the Pt loading in the samples was conducted using an inductively coupled plasma with a Perkin-Elmer plasma 8000 optical emission spectrometer (ICP-OES). All samples were dissolved using strong acid solution before being tested.

For the morphology study, the Beta materials were investigated using a Hitachi SU 1510 apparatus scanning electron microscopy (SEM), and the accelerating voltage was 20 kv. High-resolution TEM (HR-TEM) experiments were performed at 200 kV on a JEOL 2100F electron microscope.

The platinum dispersion of the samples was assessed by H_2 chemisorption at 25 °C, performed using a Finetec Finesorb-3010 instrument equipped with a TCD. Typically, 0.05 g of the sample was pretreated in a pure Ar flow (20 mL/min) at 200 °C for 0.5 h and then cooled down to 25 °C. Pulse chemisorption measurements were performed at this temperature with 10% H_2/Ar (20 mL/min).

The adsorption and desorption of formaldehyde was performed on a Finetec Finesorb-3010 instrument equipped with a thermal conductivity detector and programmed heating. In a typical run, 50 mg of sample were pre-treated in a pure He flow (15 mL/min) at 200 °C for 0.5 h and then cooled down to 25 °C prior to the adsorption of formaldehyde for 1 h. After saturation with formaldehyde, the sample was flushed with pure He (15 mL/min) for 1 h at 25 °C. The profiles of desorbed species were recorded online at a heating rate of 10 °C/min.

The acidity of the samples was measured by the temperature-programmed-desorption of ammonia (NH_3-TPD) on a Micromeritics AutoChem II 2920. The sample (0.2 g, 40–60 mesh) was pretreated at 500 °C in a N_2 flow for 60 min, followed by the adsorption of NH_3 at 100 °C for 30 min. After saturation, the sample was purged by N_2 flow for 30 min at 100 °C to remove the physically adsorbed ammonia on the sample. Then, desorption of NH_3 was carried out from 100 to 600 °C with a heating rate of 10 °C/min.

X-ray photoelectron spectra (XPS) of the samples were recorded using a Thermo ESCALAB 250 with Al *Kα* X-ray radiation for the X-ray source. The binding energies (BEs) were calibrated against C1s (285.0 eV) and Al2p (73.9 eV) peaks.

2.4. Catalytic tests

Complete oxidation of formaldehyde was performed in a continuous flow fixed-bed microreactor at the atmospheric pressure, consisting of a quartz tube (4 mm internal diameter) that was filled with the catalyst. A typical experiment was performed using a catalytic bed of 100 mg of catalyst (40–60 mesh) with total flow rate of feed stream at 100 mL/min (The feed gas composition was 400 ppm HCHO, 20% O_2, He as balance), 50% relative humidity (RH), and a space velocity (SV) of 60,000 mL/(g h). The RH of the feed gas was determined by a high accuracy thermo-hygrometer with a probe (WSB-2-H2, Zhengzhou Boyang). Gaseous HCHO was generated by

flowing He over paraformaldehyde, which was placed in a thermostatic water bath. As the same with previous activity evaluating instruments and methods [52,79], the inlet and outlet gases were monitored by FTIR (Nicolet iS50 equipped with 2 m gas cell and a DTGS detector, resolution: 0.5 cm^{-1}, OPD velocity: 0.4747 cm s^{-1}). The collected region was 600–4000 cm^{-1} and the number of scans per spectrum was 16 times. HCHO and CO_2 were measured by the peaks located at 2897 (C—H vibration) and 2350 cm^{-1} (O—C—O vibration), respectively. The CO_2 concentrations were quantified and calculated based on the peak area of CO_2 at 2350 cm^{-1}. Since no other carbon containing compounds except for CO_2 were detected in the effluents for all tested samples, the conversion was calculated from a carbon balance that 1 mol of HCHO forms 1 mol of CO_2.

Kinetic rates in oxidation of HCHO to CO_2 with H_2O and oxidation of HCOOH to CO_2 with H_2O were measured in a gaseous flowing fixed reactor, while kinetic rates in oxidation of HCHO to HCOOH were measured in a liquid reactor.

The kinetic measurements for oxidation of HCHO to CO_2 with H_2O were implemented from the HCHO conversion below 15%, HCHO concentration of 3000 ppm, GHSV at 240,000 mL/(g_{cat}·h), temperature at 25 °C, relative humidity (RH) at 50%, O_2 of 20% (He as a balance gas), and flow rate of 100 mL/min. The kinetic measurements for oxidation of HCOOH to CO_2 with H_2O were implemented from the HCOOH conversion below 15%, HCOOH concentration of 3000 ppm, GHSV at 240,000 mL/(g_{cat}·h), temperature at 25 °C, relative humidity (RH) at 50%, O_2 of 20% (He as a balance gas), and flow rate of 100 mL/min. In these measurements, HCHO, HCOOH and CO_2 were calculated from the peak intensities located at 2897 cm^{-1} (C—H vibration) for HCHO, 1340 cm^{-1} (C—H vibration) for HCOOH, and 2350 cm^{-1} (O—C—O vibration) for CO_2, respectively. Since no other carbon containing compounds except for CO_2 were detected in the effluents for all tested samples, the conversion was calculated from a carbon balance that 1 mol of HCHO forms 1 mol of CO_2 and 1 mol of HCOOH forms 1 mol of CO_2.

Kinetic measurements for oxidation of HCHO to HCOOH were implemented from the formaldehyde conversion below 5%, HCHO concentration of 0.06715 mol/L, solution volume of 50 mL, catalyst of 0.05 g, reaction temperature at 25 °C, and reaction for 5 h. The reactants and products were analyzed by a Shimadzu GC-2014 chromatograph equipped with FID detector and a Agilent HP6890 Gas chromatography-mass spectrometry.

3. Results and discussion

3.1. Catalytic performances in HCHO oxidation

Fig. 1 shows dependences of HCHO conversion on reaction temperature in HCHO oxidation over the various catalysts under HCHO concentration of 400 ppm. Before the tests, all catalysts were pretreated in flowing H_2 at 300 °C for 2 h. For the Pt/H-Beta-TEA-12 catalyst, the temperature for complete oxidation of HCHO is *ca.* 46 °C, which is very similar to the temperatures of zeolite supported Pt catalysts reported previously [69,80]. In contrast, all Pt/H-Beta-SDS catalysts show much lower temperatures for complete oxidation of HCHO under the same condition (Table S1). Neither CO nor small organic molecules could be detected in the tail gas, and CO_2 together with H_2O are the only products. Notably, the catalytic activities catalysts quantitatively improve with the decrease of the zeolite Si/Al ratios, as shown in Figs. S1–S5, which might be attributed to increasing acidic density and Pt dispersion in the catalysts. Particularly, Pt/H-Beta-SDS-4 sample exhibits room temperature (25 °C) for the complete oxidation of HCHO.

Fig. 2 shows the dependences of the conversion on the reaction time of HCHO oxidation over the Pt/H-Beta-SDS-4 under an initial HCHO concentration ranging from 80 to 800 ppm at 25 °C.

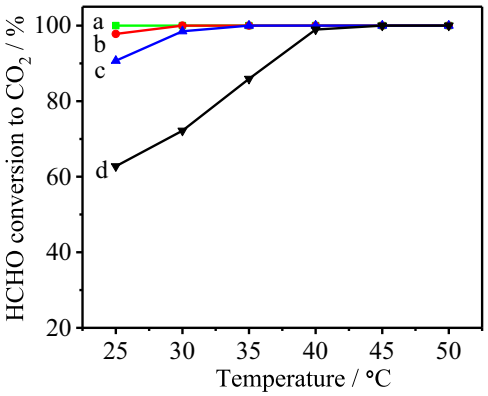

Fig. 1. Dependences of HCHO conversion on reaction temperature in HCHO oxidation over the (a) Pt/H-Beta-SDS-4, (b) Pt/H-Beta-SDS-8, (c) Pt/H-Beta-SDS-10, and (d) Pt/H-Beta-TEA-12 catalysts under HCHO concentration of 400 ppm, O_2 20%, rate of 100 mL/min, space velocity of 60000 mL/g·h, relative humidity of 50%, and He as the balance gas.

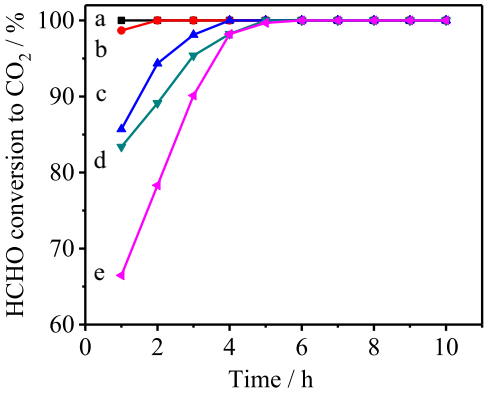

Fig. 2. Dependences of HCHO conversion on reaction time with initial HCHO concentration of (a) 80, (b) 200, (c) 400, (d) 600, and (e) 800 ppm in the HCHO oxidation over the Pt/H-Beta-SDS-4 catalyst under O_2 20 vol% (He as a balance gas), total flow rate 100 cm^3/min, relative humidity (RH) at 50%, SV = 60,000 mL/(g·h), and temperature at 25 °C.

Evidently, HCHO at various concentrations could be completely oxidized into CO_2, but a higher initial concentration requires a longer time to achieve the full oxidation of HCHO (100%). When the space velocity of the reaction is increased from 60000 mL/g h to 240000 mL/g h, the Pt/H-Beta-SDS-4 still gives a complete oxidation of HCHO (Fig. S6). If the relative humidity is changed to higher than 90%, the Pt/H-Beta-SDS-4 needs much less time to reach the complete oxidation of HCHO at room temperature (Fig. S7). In contrast, if H_2O is absent in the system, the sample shows relatively lower activity. Fig. 3 shows dependences of catalytic activity and selectivity on reaction time under HCHO concentrations of 400 ppm and 5000 ppm, respectively. When the HCHO concentration is 400 ppm, the Pt/H-Beta-SDS-4 Exhibits 100% HCHO conversion and CO_2 selectivity. When the HCHO concentration reaches 5000 ppm, the conversion reduces to 35%, but the selectivity still remains 100% over the Pt/H-Beta-SDS-4. These results demonstrate that the Pt/H-Beta-SDS-4 sample is highly active, very selective, and extraordinarily durable for the complete oxidation of HCHO at room temperature.

Fig. S8 shows the dependences of HCHO conversion on reaction temperature in HCHO oxidation over the Pt/H-Beta-SDS-4 samples pretreated at various temperatures under flowing hydrogen under HCHO concentration of 400 ppm, and their complete oxidation temperature for HCHO are summarized in Table S2. Apparently, Pt/H-Beta-SDS sample pretreated in flowing H_2 at 300 °C is suit-

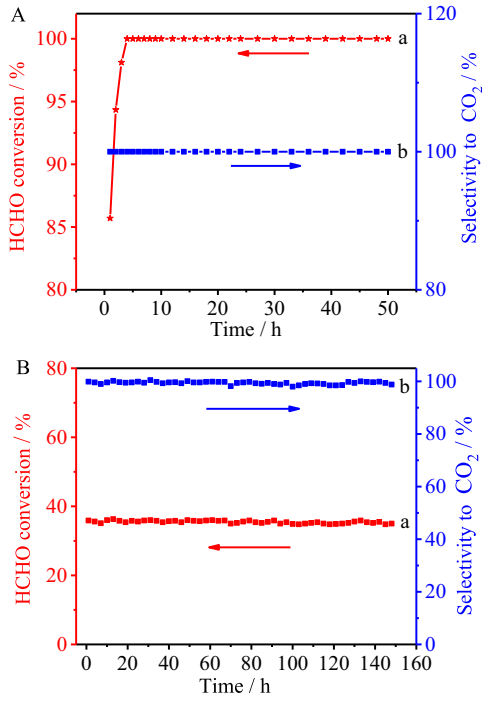

Fig. 3. Dependence of activities on reaction time in HCHO conversion (a) and selectivity to CO_2 (b) over Pt/H-Beta-SDS-4 catalyst under the conditions of HCHO concentration at (A) 400 ppm and (B) 5000 ppm, O_2 concentration of 20 vol%, He as balance, total flow rate of 100 cm^3/min, relative humidity (RH) at 50%, space velocity of 60,000 mL/(g h), and reaction temperature at 25 °C.

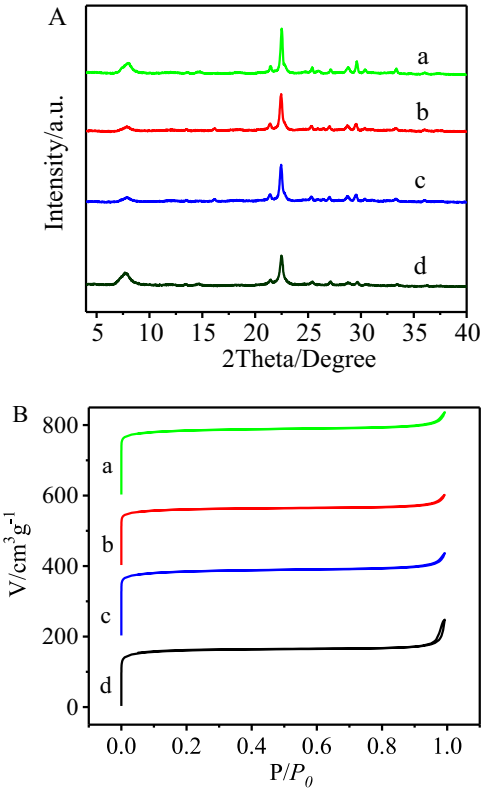

Fig. 4. (A) XRD patterns, and (B) N_2 sorption isotherms of (a) Pt/H-Beta-SDS-4, (b) Pt/H-Beta-SDS-8, (c) Pt/H-Beta-SDS-10, and (d) Pt/H-Beta-TEA-12 catalysts. The isotherms (a)–(c) in Fig. 4B have been off-set by 600, 400, and 200 cm^3/g at the beginning for clarity, respectively.

able for complete oxidation of HCHO at room temperature, which might be related to the valence state of Pt species in the catalysts.

Fig. S9 shows the Pt4d XPS spectra of as-synthesized Pt/H-Beta-SDS-4 and this sample pretreated at 200, 300, and 400 °C. After deconvolution [81,82], the proportions of Pt^0, denoted as $P(Pt^0)$, in these samples could be estimated, as presented in Table S3. Interestingly, the Pt^0 concentration pretreated at 300 °C was 57%; there is almost no change in the Pt^0 concentration for pretreated temperature from 300 °C to 400 °C. Therefore, the pretreatment in flowing H_2 at 300 °C is suitable for complete oxidation of HCHO at room temperature, where relatively high Pt^0 concentration in the samples has been achieved. These results suggest that the control of Pt valence state in the samples is a critical factor for HCHO oxidation.

3.2. Catalyst characterizations

Fig. 4 shows XRD pattern and N_2 sorption isotherms of the Pt/H-Beta catalysts with various Si/Al ratios. As shown in Fig. 4A, XRD patterns of the H-Beta-SDS-4, H-Beta-SDS-8, H-Beta-SDS-10, and H-Beta-TEA-12 supported noble metal Pt samples exhibited well-resolved characteristic peaks associated with Beta zeolite structure but the introduction of Pt did not induce the appearances of the peaks of polycrystalline noble metals, which indicates that the Pt are in very high dispersion degree on the samples. Fig. 4B shows N_2 sorption isotherms of all samples, giving very similar curves below the relative pressure (P/P_0) of 0.95. As a result, both samples exhibit very similar BET surface areas and micropore volumes, as presented in Table 1. In addition, the SEM images of all samples show that they have almost the same crystal sizes, as given in Fig. 5. Considering that the all samples have almost the same textural parameters (Fig. 4 and Table 1) and zeolite crystal sizes (Fig. 5), it is proposed that the difference in their catalytic activities might be resulted from their distinguishable Pt nanoparticles and acidic density.

Fig. 6 shows HRTEM images and Pt nanoparticle size distribution of the Pt/H-Beta catalysts with various Si/Al ratios. Interestingly, the Pt size distribution of Pt/H-Beta-SDS-4 is clearly smaller than those of other samples, as confirmed by the estimation of platinum dispersion from H_2 chemisorption (Table 1). Interestingly, the platinum dispersion significantly enhances with the decrease of the zeolite Si/Al ratio, as shown in Fig. S10. This phenomenon might be related to the H-Beta-SDS-4 having more negative charge in the zeolite framework than other samples, which should be favorable for the interaction of positively charged Pt with the negatively charged zeolite framework, leading to higher Pt dispersion in the sample, in good agreement with results reported previously [72,73].

The acidic density of the Pt/H-Beta catalysts with various Si/Al ratios has been investigated by NH_3-TPD technique [74,76], as shown in Fig. S11. The results indicate that the acidic density effectively increases with Al amount in the catalysts. Because the Pt/H-Beta-SDS-4 has more 4-coordinative Al^{3+} in the zeolite framework than the other catalysts, the Pt/H-Beta-SDS-4 exhibits much higher acidic density than the other samples. High acidic density in the Pt/H-Beta-SDS-4 is perhaps beneficial to the activation of HCHO reactant, possibly due to the relatively strong interaction of HCHO molecules with acidic species of the zeolite. This explanation is evidently supported by the adsorption of HCHO (HCHO-TPD), followed by the programmed desorption of the samples, where the Pt/H-Beta-SDS-4 shows much stronger signal intensity than the other samples (Fig. 7).

3.3. Kinetic studies

To understand the higher activity in the HCHO oxidation over the Pt/H-Beta-SDS-4 than that over the other sample, the reactant

Table 1
Textural parameters of the Pt/H-Beta-SDS-4, Pt/H-Beta-SDS-8, Pt/H-Beta-SDS-10, and Pt/H-Beta-TEA-12 samples.

Catalyst	Si/Al[a]	Pt[a] (wt%)	BET[b] m^2/g	V^b_{micro} cm^3/g	Platinum dispersion[c] (%)
Pt/H-Beta-SDS-4	4.28	0.976	541	0.25	45
Pt/H-Beta-SDS-8	7.88	0.985	532	0.23	41
Pt/H-Beta-SDS-10	10.12	0.994	539	0.24	36
Pt/H-Beta-TEA-12	11.67	0.989	540	0.24	33

[a] Determined from the ICP-OES analysis.
[b] Determined from the N_2 sorption isotherms.
[c] Determined from H_2 chemisorption.

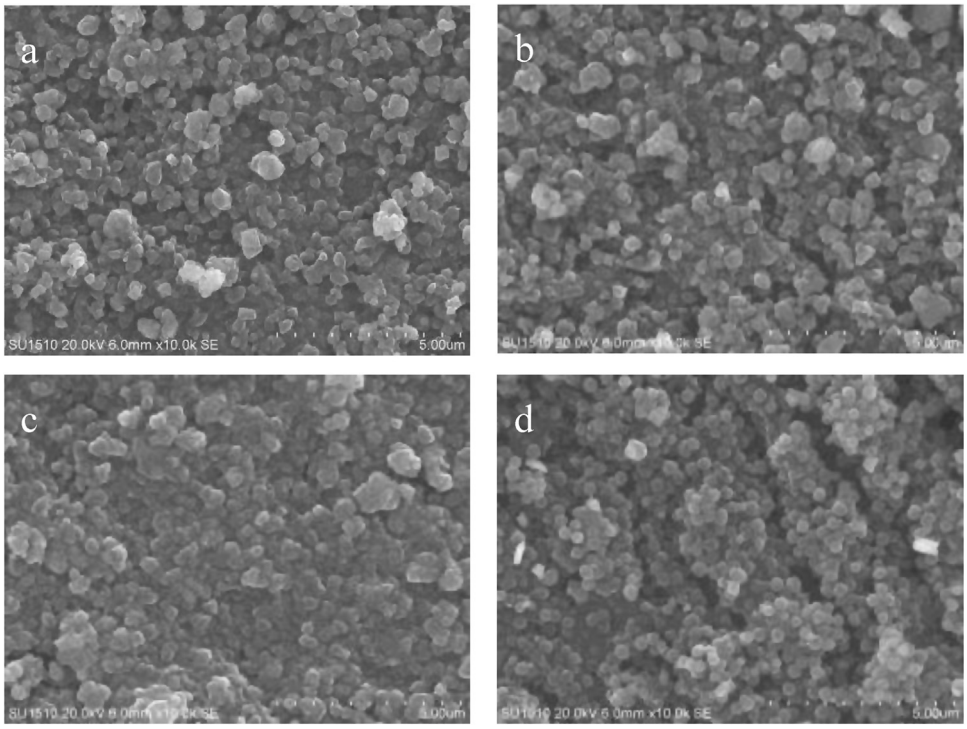

Fig. 5. SEM images of the (a) Pt/H-Beta-SDS-4, (b) Pt/H-Beta-SDS-8, (c) Pt/H-Beta-SDS-10, and (d) Pt/H-Beta-TEA-12 catalysts.

Table 2
Reactant order in the HCHO oxidation over the Pt/H-Beta-SDS and Pt/H-Beta-TEA samples.

Catalyst	HCHO order	Oxygen order
Pt/H-Beta-SDS-4	0.711	1.302
Pt/H-Beta-SDS-8	0.720	1.336
Pt/H-Beta-SDS-10	0.729	1.361
Pt/H-Beta-TEA-12	0.731	1.385

order of HCHO and oxygen has been investigated according to the equation in the following:

$$\ln R = x\ln[A] + \text{constant}$$

where R is the reaction rate, [A] is the reactant concentration, and x is the reactant order. The x could be obtained from the slope of a graph of lnR as a function of ln[A], as calculated in Fig. 8 and presented in Table 2. Notably, compared with the other samples, the order of both HCHO and oxygen over the Pt/H-Beta-SDS-4 is significantly reduced. The reduction of the oxygen order should be assigned to improved Pt dispersion, while the decrease of HCHO order could be attributed to increased acidic density in the samples. The dependences of the reactant order on the Pt dispersion or Si/Al ratio are given in Figs. S12 and S13 . Higher Pt dispersion should result in a larger oxygen adsorption capacity, improving the reaction rate. As a result, the oxygen order should be reduced. At the same time, higher acidic density should be favorable for the adsorption of HCHO molecules, enhancing the reaction rate. These results strongly support the design strategies for enhancing activity over zeolite-supported noble metal samples in the complete oxidation of HCHO at low temperatures, particularly room temperature.

Generally, the complete oxidation of HCHO mainly involves (i) oxidation of HCHO to formate species, (ii) decomposition of the formate species, and (iii) formation of CO_2 and H_2O by oxidation of the decomposed species [50,51]. The combination of step (ii) and step (iii) could be considered the oxidation of HCOOH to CO_2 and H_2O. In the case of a titania-supported Pt sample with sodium modifications (Na-Pt/TiO_2, one of the most active for the complete oxidation of HCHO), the decomposition of the formate species is regarded as the rate-determining step, where the additive such as sodium species play a critical role in the complete oxidation of HCHO at room temperature [43–45,48,50,53]. According to this idea, we have rationally prepared Pt/Beta-SDS-4 samples with modified alkali cations (Na^+ or K^+), which have been denoted as Pt/Na-Beta-SDS-4 and Pt/K-Beta-SDS-4, respectively. Although the Pt/Na-Beta-SDS-4 and Pt/K-Beta-SDS-4 samples have very similar crystallinity, Si/Al ratios, and Pt loading to those of the Pt/H-Beta-SDS-4 (Figs. 9 and S14–S16 and Table S4), they exhibit much lower activities than the Pt/H-Beta-SDS-4, as shown in Fig. S17. The temperature for complete oxidation of HCHO over Pt/Na-Beta-

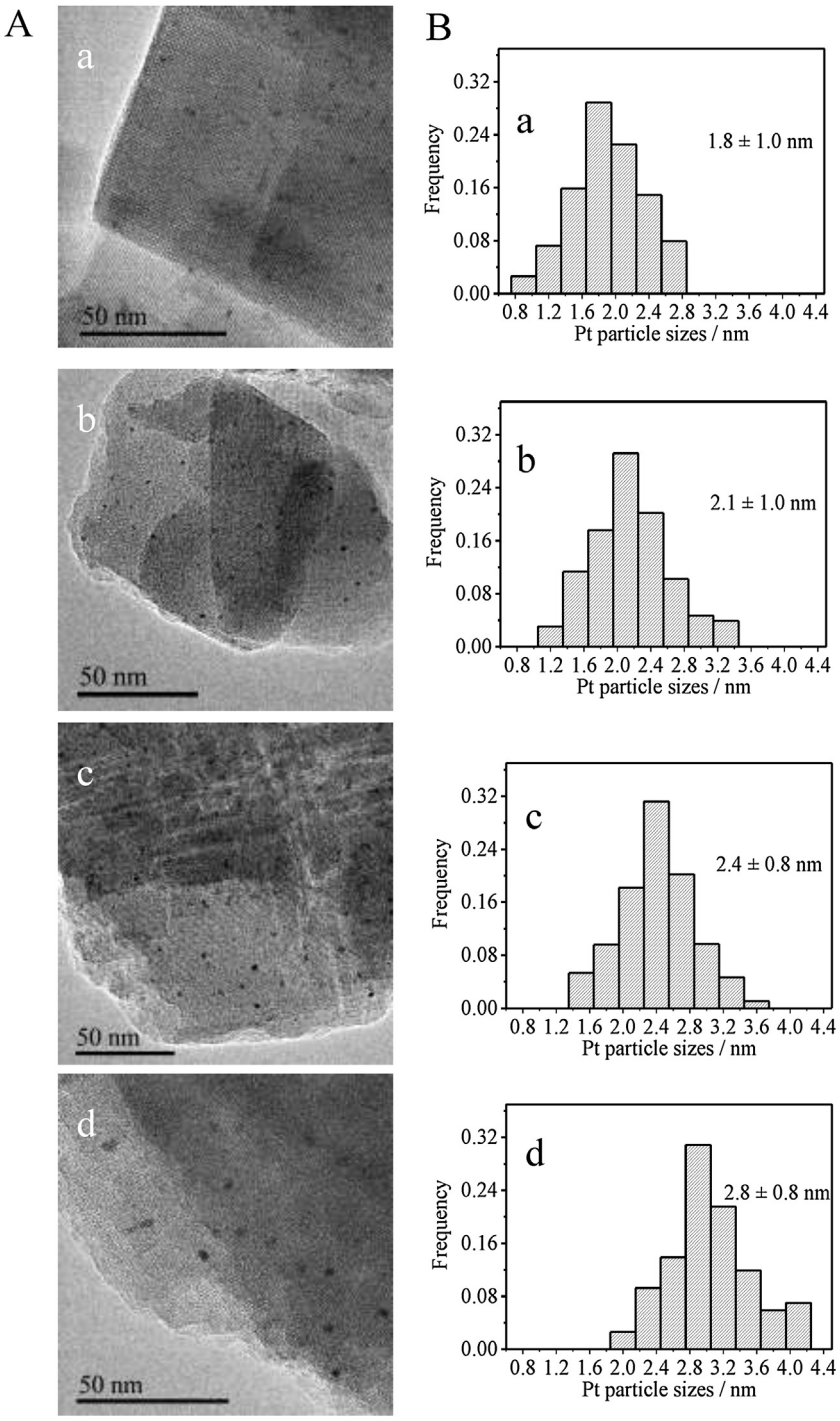

Fig. 6. (A) HRTEM images and (B) Pt particle size distribution of (a) Pt/H-Beta-SDS-4, (b) Pt/H-Beta-SDS-8, (c) Pt/H-Beta-SDS-10, and (d) Pt/H-Beta-TEA-12 catalysts.

SDS-4 and Pt/K-Beta-SDS-4 exceeds 140 °C. These results indicate that alkali cations are not suitable promoters of HCHO oxidation in zeolite-supported noble metal catalysts. These results also suggest that the mechanism on the HCHO oxidation over the Pt/H-Beta-SDS-4 is quite different from that of conventional Na-Pt/TiO_2 catalyst [50].

To understand a key step in the HCHO oxidation over the zeolite-supported Pt catalysts, we have systematically investigated the kinetic rates of oxidation of HCHO to CO_2 (r_0), oxidation of HCHO to HCOOH (r_1), and oxidation of HCOOH into CO_2 (r_2) over the all catalysts, as given in Figs. 10 and S18–S19. Notably, the r_2 values of all samples are larger than their r_0 and r_1 values, indicating that the key step for the complete oxidation of HCHO over the zeolite Beta supported noble samples should be the oxidation of HCHO to HCOOH, rather than the oxidation of HCOOH to CO_2. Particularly, in these Pt/H-Beta catalysts, the r_1 values significantly increase with the decrease of the Si/Al ratios, which is strongly related to the acidic contribution for the conversion of HCHO to HCOOH. This feature is quite different from the results obtained from the Na-Pt/TiO_2 sample [50]. In the Na-Pt/TiO_2 catalyzed HCHO oxidation, the rate of HCOOH to CO_2 is effectively enhanced. In contrast, in the Pt/H-Beta-SDS-4 catalyzed HCHO oxidation, the rate of HCHO

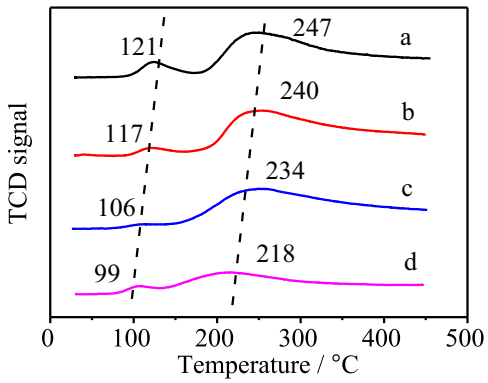

Fig. 7. HCHO-TPD curves of (a) Pt/H-Beta-SDS-4, (b) Pt/H-Beta-SDS-8, (c) Pt/H-Beta-SDS-10, and (d) Pt/H-Beta-TEA-12 catalysts.

to HCOOH is significantly improved. In addition, the replacement of alkali cations with protons in these zeolite-supported Pt catalysts remarkably enhances the activity, confirming the important contribution of acidic sites for oxidation of HCHO to HCOOH. These data are well consistent with those of the oxidation of glycerol over the zeolite-based Pt catalysts, where the high acidic density is favorable for the activation of oxygenates [71].

4. Conclusion

In summary, Al-rich Beta zeolite supported Pt sample (Pt/H-Beta-SDS-4) exhibits high activity, excellent selectivity for CO_2, and extraordinary durability in the complete oxidation of HCHO at room temperature, which is very important for the removal of indoor air pollutants. The superior properties of this sample result from the comprehensive contribution of highly dispersed Pt nanoparticles and a high density of acidic sites, which are related to the choice of Al-rich Beta zeolite support, where the abundant aluminum species in the zeolite framework not only improve the high acidic density but also enhance the interaction of positively charged noble metals and the negatively charged zeolite framework. The strategy of designing zeolite-supported noble metal catalysts might offer an alternative way to develop highly efficient heterogeneous catalysts for the removal of air pollutants.

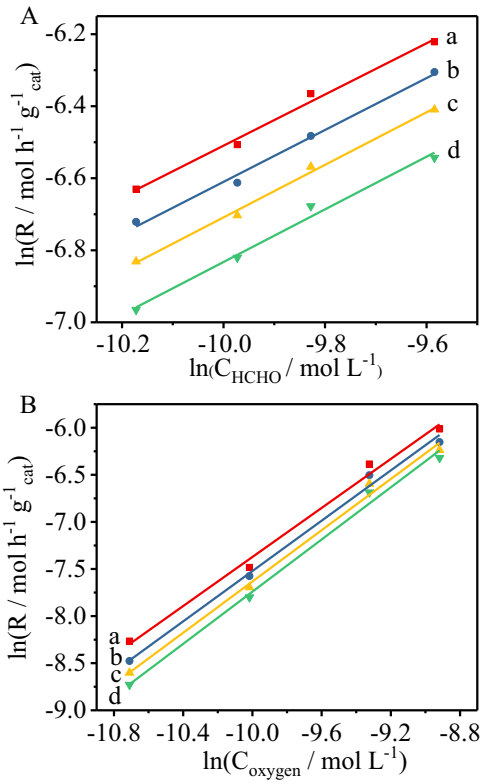

Fig. 8. Estimation of (A) HCHO and (B) oxygen orders from the dependence of kinetic rate on the reactant concentration in the HCHO oxidation over the (a) Pt/H-Beta-SDS-4, (b) Pt/H-Beta-SDS-8, (c) Pt/H-Beta-SDS-10, and (d) Pt/H-Beta-TEA-12 catalysts.

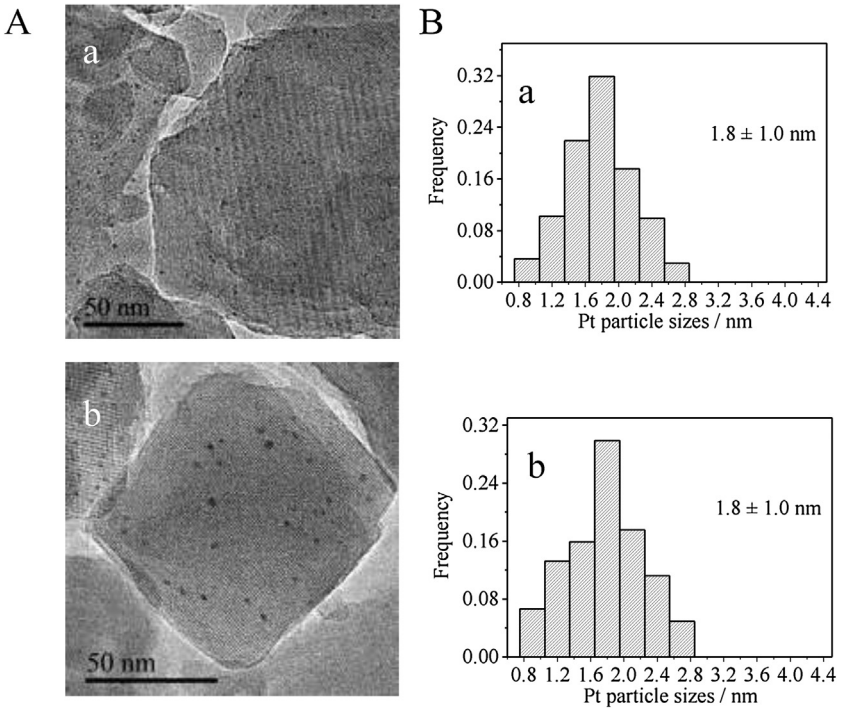

Fig. 9. (A) HR-TEM images and (B) Pt particle size distribution of (c) Pt/Na-Beta-SDS-4 and (d) Pt/K-Beta-SDS-4 samples.

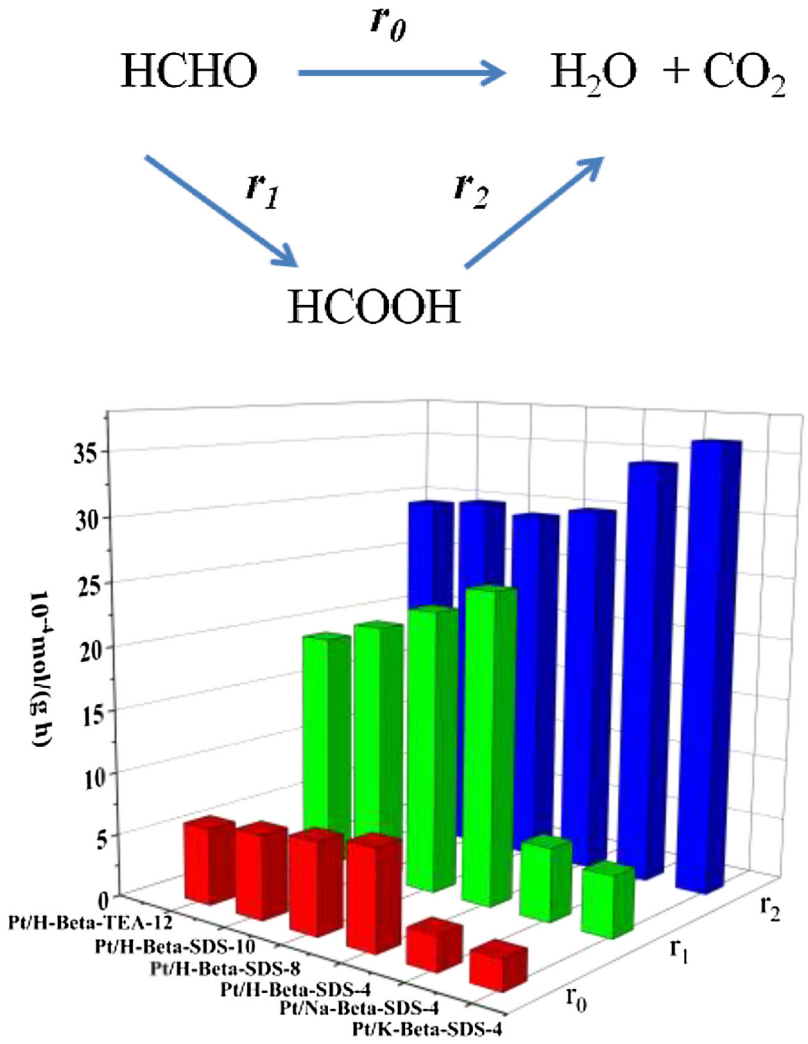

Fig. 10. Kinetic rates of oxidation of HCHO to CO_2 and H_2O, oxidation of HCHO to HCOOH, and oxidation of HCOOH to CO_2 and H_2O over various Pt/Beta catalysts.

Acknowledgments

This work is supported by the National Natural Science Foundation of China (21673205, 21333009 and 21422306) and the Zhejiang Provincial Natural Science Foundation of China (Grant Nos. LR15B030001 and LY16B030004).

Appendix A. Supplementary data

Supplementary data associated with this article can be found, in the online version, at http://dx.doi.org/10.1016/j.apcatb.2017.07.015.

References

[1] A.P. Jones, Atmos. Environ. 33 (1999) 4535–4564.
[2] C. Yu, D. Crump, Build. Environ. 33 (1998) 357–374.
[3] T. Salthammer, S. Mentese, R. Marutzky, Chem. Rev. 110 (2010) 2536–2572.
[4] B.Y. Bai, Q. Qiao, J.H. Li, J.M. Hao, Chin. J. Catal. 37 (2016) 102–122.
[5] B.Y. Bai, Q. Qiao, H. Arandiyan, J.H. Li, J.M. Hao, Environ. Sci. Technol. 50 (2016) 2635–2640.
[6] D.W. Kwon, P.W. Seo, G.J. Kim, S.C. Hong, Appl. Catal. B Environ. 163 (2015) 436–443.
[7] J. Wang, P. Zhang, J. Li, C. Jiang, R. Yunus, J. Kim, Environ. Sci. Technol. 49 (2015) 12372–12379.
[8] Q. Xu, W. Lei, X. Li, X. Qi, J. Yu, G. Liu, J. Wang, P. Zhang, Environ. Sci. Technol. 48 (2014) 9702–9708.
[9] X.J. Tang, Y. Bai, A. Duong, M.T. Smith, L.Y. Li, L.P. Zhang, Environ. Int. 35 (2009) 1210–1224.
[10] J.J. Collins, R. Ness, R.W. Tyl, N. Krivanek, N.A. Esmen, T.A. Hall, Regul Toxicol. Pharm. 34 (2001) 17–34.
[11] J. Wang, J. Li, C. Jiang, P. Zhou, P. Zhang, J. Yu, Appl. Catal. B Environ. 204 (2017) 147–155.
[12] Z. Xu, J. Yu, M. Jaroniec, Appl. Catal. B Environ. 163 (2015) 306–312.
[13] Z. Yan, Z. Xu, J. Yu, M. Jaroniec, Appl. Catal. B Environ. 199 (2016) 458–465.
[14] T. Yang, Y. Huo, Y. Liu, Z. Rui, H. Ji, Appl. Catal. B Environ. 200 (2017) 543–551.
[15] H.Q. Rong, Z.Y. Liu, Q.L. Wu, D. Pan, J.T. Zheng, Cellulose 17 (2010) 205–214.
[16] J.J. Pei, J.S.S. Zhang, Chem. Eng. J. 167 (2011) 59–66.
[17] Y.S. Tao, H. Kanoh, L. Abrams, K. Kaneko, Chem. Rev. 106 (2006) 896–910.
[18] J.P. Bellat, I. Bezverkhyy, G. Weber, S. Royer, R. Averlant, J.M. Giraudon, J.F. Lamonier, J. Hazard. Mater. 300 (2015) 711–717.
[19] P.A. Bourgeois, E. Puzenat, L. Peruchon, F. Simonet, D. Chevalier, E. Deflin, C. Brochier, C. Guillard, Appl. Catal. B Environ. 128 (2012) 171–178.
[20] Y.W. Lu, D.H. Wang, C.F. Ma, H.C. Yang, Build. Environ. 45 (2010) 615–621.
[21] F. Shiraishi, D. Ohkubo, K. Toyoda, S. Yamaguchi, Chem. Eng. J. 114 (2005) 153–159.
[22] S.B. Wang, H.M. Ang, M.O. Tade, Environ. Int. 33 (2007) 694–705.
[23] T. Noguchi, A. Fujishima, Environ. Sci. Technol. 32 (1998) 3831–3833.
[24] G. Qin, Y. Zhang, X. Ke, X. Tong, Z. Sun, M. Liang, S. Xue, Appl. Catal. B Environ. 129 (2013) 599–605.
[25] Y. Huang, B. Long, M. Tang, Z. Rui, M.-S. Balogun, Y. Tong, H. Ji, Appl. Catal. B Environ. 181 (2016) 779–787.
[26] B.Y. Dong, S.R. Lan, J. Phys. Conf. Ser. (2013) 418.
[27] X. Zhu, X. Gao, R. Qin, Y. Zeng, R. Qu, C. Zheng, X. Tu, Appl. Catal. B Environ. 170–171 (2015) 293–300.
[28] D.Z. Zhao, X.S. Li, C. Shi, H.Y. Fan, A.M. Zhu, Chem. Eng. Sci. 66 (2011) 3922–3929.
[29] M.B. Chang, C.C. Lee, Environ. Sci. Technol. 29 (1995) 181–186.
[30] B.Y. Bai, H. Arandiyan, J.H. Li, Appl. Catal. B Environ. 142 (2013) 677–683.
[31] C. Shi, Y. Wang, A.M. Zhu, B.B. Chen, C. Au, Catal. Commun. 28 (2012) 18–22.
[32] C. Shi, B.B. Chen, X.S. Li, M. Crocker, Y. Wang, A.M. Zhu, Chem. Eng. J. 200 (2012) 729–737.

[33] D.Z. Zhao, T.Y. Ding, X.S. Li, J.L. Liu, C.A. Shi, A.M. Zhu, Chin. J. Catal. 33 (2012) 396–401.
[34] D.Z. Zhao, C. Shi, X.S. Li, A.M. Zhu, B.W.L. Jang, J. Hazard. Mater. 239 (2012) 362–369.
[35] B.B. Chen, C. Shi, M. Crocker, Y. Wang, A.M. Zhu, Appl. Catal. B Environ. 132–133 (2013) 245–255.
[36] B.B. Chen, X.B. Zhu, M. Crocker, Y. Wang, C. Shi, Appl. Catal. B Environ. 154–155 (2014) 73–81.
[37] P. Liu, H. He, G. Wei, X. Liang, F. Qi, F. Tan, W. Tan, J. Zhu, R. Zhu, Appl. Catal. B Environ. 182 (2016) 476–484.
[38] T. Chen, H.Y. Dou, X.L. Li, X.F. Tang, J.H. Li, J.M. Hao, Microporous Mesoporous Mater. 122 (2009) 270–274.
[39] S. Imamura, D. Uchihori, K. Utani, T. Ito, Catal. Lett. 24 (1994) 377–384.
[40] X.F. Tang, J.H. Li, J.M. Hao, Catal. Commun. 11 (2010) 871–875.
[41] X.F. Tang, Y.G. Li, X.M. Huang, Y.D. Xu, H.Q. Zhu, J.G. Wang, W.J. Shen, Appl. Catal. B Environ. 62 (2006) 265–273.
[42] Y.R. Wen, X. Tang, J.H. Li, J.M. Hao, L.S. Wei, X.F. Tang, Catal. Commun. 10 (2009) 1157–1160.
[43] C.B. Zhang, H. He, K. Tanaka, Catal. Commun. 6 (2005) 211–214.
[44] C.B. Zhang, H. He, K. Tanaka, Appl. Catal. B Environ. 65 (2006) 37–43.
[45] C.B. Zhang, H. He, Catal. Today 126 (2007) 345–350.
[46] X. Tang, J. Chen, X. Huang, Y. Xu, W. Shen, Appl. Catal. B Environ. 81 (2008) 115–121.
[47] J. Xu, T. White, P. Li, C.H. He, Y.F. Han, J. Am. Chem. Soc. 132 (2010) 13172–13173.
[48] H.B. Huang, D.Y.C. Leung, ACS Catal. 1 (2011) 348–354.
[49] Z. Huang, X. Gu, Q. Cao, P. Hu, J. Hao, J. Li, X. Tang, Angew. Chem. 51 (2012) 4198–4203.
[50] C. Zhang, F. Liu, Y. Zhai, H. Ariga, N. Yi, Y. Liu, K. Asakura, M. Flytzani-Stephanopoulos, H. He, Angew. Chem. 51 (2012) 9628–9632.
[51] L.H. Nie, J.G. Yu, X.Y. Li, B. Cheng, G. Liu, M. Jaroniec, Environ. Sci. Technol. 47 (2013) 2777–2783.
[52] J.Q. Torres, S. Royer, J.P. Bellat, J.M. Giraudon, J.F. Lamonier, ChemSusChem 6 (2013) 578–592.
[53] C.B. Zhang, Y.B. Li, Y.F. Wang, H. He, Environ. Sci. Technol. 48 (2014) 5816–5822.
[54] J.H. Zhang, Y.B. Li, L. Wang, C.B. Zhang, H. He, Catal. Sci. Technol. 5 (2015) 2305–2313.
[55] X.L. Liang, P. Liu, H.P. He, G.L. Wei, T.H. Chen, W. Tan, F.D. Tan, J.X. Zhu, R.L. Zhu, J. Hazard. Mater. 306 (2016) 305–312.
[56] J.X. Peng, S.D. Wang, Appl. Catal. B Environ. 73 (2007) 282–291.
[57] L.H. Nie, J.G. Yu, J.W. Fu, ChemCatChem 6 (2014) 1983–1989.
[58] L.H. Nie, P. Zhou, J.G. Yu, M. Jaroniec, J. Mol. Catal. A Chem. 390 (2014) 7–13.
[59] L.F. Qi, B. Cheng, J.G. Yu, W.K. Ho, J. Hazard. Mater. 301 (2016) 522–530.
[60] M.C. Alvarez-Galvan, V.A.D.P. O'Shea, J.L.G. Fierro, P.L. Arias, Catal. Commun. 4 (2003) 223–228.
[61] M.C. Alvarez-Galvan, B. Pawelec, V.A.D. O'Shea, J.L.G. Fierro, P.L. Arias, Appl. Catal. B Environ. 51 (2004) 83–91.
[62] V.A.D.P. O'Shea, M.C. Alvarez-Galvan, J.L.G. Fierro, P.L. Arias, Appl. Catal. B Environ. 57 (2005) 191–199.
[63] C.F. Mao, M.A. Vannice, J. Catal. 154 (1995) 230–244.
[64] Z.P. Qu, S.J. Shen, D. Chen, Y. Wang, J. Mol. Catal. A Chem. 356 (2012) 171–177.
[65] N.H. An, W.L. Zhang, X.L. Yuan, B. Pan, G. Liu, M.J. Jia, W.F. Yan, W.X. Zhang, Chem. Eng. J. 215 (2013) 1–6.
[66] A. Corma, Chem. Rev. 95 (1995) 559–614.
[67] A. Corma, Chem. Rev. 97 (1997) 2373–2419.
[68] M.E. Davis, Nature 417 (2002) 813–821.
[69] S.J. Park, I. Bae, I.S. Nam, B.K. Cho, S.M. Jung, J.H. Lee, Chem. Eng. J. 195 (2012) 392–402.
[70] L. Zhang, Y.X. Peng, J. Zhang, L. Chen, X.J. Meng, F.S. Xiao, Chin. J. Catal. 37 (2016) 800–809.
[71] A. Villa, G.M. Veith, L. Prati, Angew. Chem. Int. Ed. 49 (2010) 4499–4502.
[72] A. Corma, A. Martinez, V. MartinezSoria, J. Catal. 169 (1997) 480–489.
[73] S.J. Tauster, S.C. Fung, R.T.K. Baker, J.A. Horsley, Science 211 (1981) 1121–1125.
[74] B. Xie, H.Y. Zhang, C.G. Yang, S.Y. Liu, L.M. Ren, L. Zhang, X.J. Meng, B. Yilmaz, U. Muller, F.-S. Xiao, Chem. Commun. 47 (2011) 3945–3947.
[75] B. Xie, J.W. Song, L.M. Ren, Y.Y. Ji, J.X. Li, F.-S. Xiao, Chem. Mater. 20 (2008) 4533–4535.
[76] S. Suganuma, H.Y. Zhang, C.G. Yang, F.S. Xiao, N. Katada, J. Porous Mater. 23 (2016) 415–421.
[77] H.Y. Zhang, B. Xie, X.J. Meng, U. Muller, B. Yilmaz, M. Feyen, S. Maurer, H. Gies, T. Tatsumi, X.H. Bao, W.P. Zhang, D. De Vos, F.-S. Xiao, Microporous Mesoporous Mater. 180 (2013) 123–129.
[78] C. Chen, Q. Wu, F. Chen, L. Zhang, S. Pan, C. Bian, X. Zheng, X. Meng, F.-S. Xiao, J. Mater. Chem. A 3 (2015) 5556–5562.
[79] J. Zhang, Y. Li, Y. Zhang, M. Chen, L. Wang, C. Zhang, H. He, Sci. Rep. 5 (2015) 12950.
[80] H.Y. Chen, Z.B. Rui, X.Y. Wang, H.B. Ji, Catal. Today 258 (2015) 56–63.
[81] D. Ghita, P. Rosca, D.S. Ezeanu, Rev. Chim-Bucharest 63 (2012) 1056–1061.
[82] S. Damyanova, J.M.C. Bueno, Appl. Catal. A-Gen. 253 (2003) 135–150.